Annals of the BMVA Vol. 2013, No. 6, pp 1–14 (2013)

Learning Dynamical Shape Prior for Level Set based Cell Tracking

Yan Nei Law[1], Hwee Kuan Lee[1] and Andy M. Yip[2]

[1] Imaging Informatics Division, Bioinformatics Institute, Singapore 138671
[2] Department of Mathematics, National University of Singapore, Singapore 119076
⟨lawyn@bii.a-star.edu.sg⟩

Abstract

Automated cell tracking in populations is very crucial for studying dynamic cell cycle behaviors. However, a high accuracy of each step is essential to avoid error propagation. In this paper, we propose an integrated three-component system to tackle this problem. We first model the temporal dynamics of shape change using an autoregressive model, which is used for estimating the shape and the location of the current object. We then segment the cell using an active contour model starting from the predicted shape. Finally, we identify its phase using a Markov model. The phase information is also used for fine-tuning the segmentation result. We applied this approach for tracking HeLa H2B-GFP cells and tested it in different aspects. Highly accurate validation results confirm the usefulness of our integrating approach and show its robustness and the essentiality of each component.

1 Introduction

Individual cell tracking from cell populations is a crucial step to obtain quantitative measurements for studying dynamic cell cycle behaviors [Lodish et al., 2000]. This is especially important when the measurements averaged over cell populations are not sufficient for detecting stochastic and transient phenotypes. For instance, in a study of a tumor suppressor p53 and its negative regulator mdm2 [Lahav et al., 2004], protein levels in each single cell were measured to illustrate the oscillation mechanism of the p53-mdm2 feedback loop. In cancer studies, cell cycle analysis provides direct information on the inappropriate cell proliferation caused by cancer disease. In many of these studies, the analysis was carried manually when the sample size was manageable. However, it is still very time-consuming and the results can be subjective. As the use of high-throughput imaging becomes popular, it is essential to automate the process of tracking individual cells from a large amount of images in an accurate, practical, and robust manner.

Although many cell tracking algorithms have been proposed and produced reasonably good results, they are often ad-hoc and may not work with other data sets. It is because the

dynamic cell cycle behavior is too complex. Firstly, the shape of a cell changes dramatically throughout the cell division process which makes it difficult to track. Secondly, the experimental settings such as data acquisition rate, noise level carried out in different laboratories can be very different.

Numerous works for cell tracking can be found in the literature [Zhou and Wong, 2006]. Since the problem can be divided into the subproblems of cell segmentation, cell tracking, and phase identification, a natural approach is to treat these subproblems separately. A lot of previous works along this line can be found. For instance, [Chen et al., 2006, Zhou et al., 2009, Li et al., 2010b] proposed to first segment the cells frame-by frame and then track the cells by associating the segmented objects. Some useful shape and context features for phase identification have been proposed in [Chen et al., 2006, Zhou et al., 2009]. However, these methods have many parameters which depend heavily on the data. They need to be tuned empirically by the users. The generality of these methods is questionable. In contrast to most existing methods that treat the subproblems separately, some methods that take a holistic view have been proposed. Indeed, this approach is more intuitive as the cell cycle is a series of events taken place inside a single cell. For instance, a level-set based algorithm has been proposed in [Dzyubachyk et al., 2010]. The algorithm performs simultaneous segmentation and tracking. For tracking purpose, the information from the previous time step is directly used to segment the cell in the current frame. However, this approach only works for limited cases and cannot handle the case when the cells move too fast.

To tackle the problem, we introduce a new system for individual cell tracking in this paper. The system shown in Fig. 1 consists of three components: (C1) Learning shape prior for tracking, (C2) Segmentation using prior, and (C3) Cell phase identification. In contrast to most of the existing methods that treat these subproblems separately, our approach treats them as one whole process, which allows the use of available biological prior knowledge for improving the performance of the whole process. This work builds upon the earlier work reported in [Law and Lee, 2012].

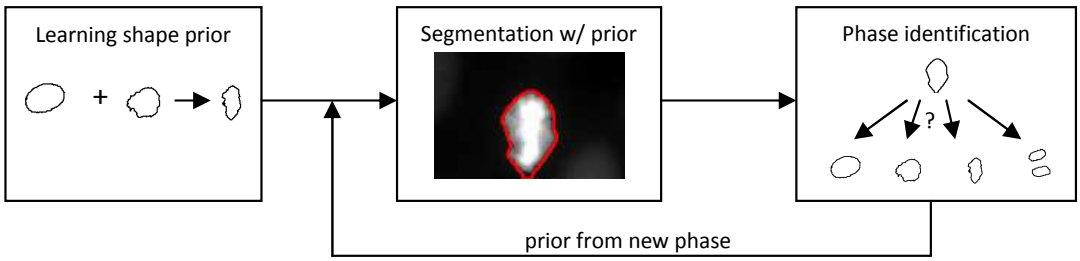

Figure 1: Flowchart of the proposed system.

For (C1), we model the temporal dynamics of shape change using an autoregressive model [Cremers, 2006]. To obtain a more reliable model, we use a low-dimensional formulation to represent a shape. The model is used for estimating the shape and the location of the current object. For (C2), we use (C1) for initialization and segment the cell using an active contour model [Li et al., 2010a]. This step greatly improves the segmentation accuracy. For (C3), we model phase transition using a Markov process and classify the segmented cell based on its shape and context features proposed in [Chen et al., 2006, Zhou et al., 2009]. If the cell undergoes a phase transition, we repeat the segmentation step with the sample shape of the new phase as an initial guess. With this biological prior knowledge, the segmentation

result is further improved. Note that our approach is very generic and can be applied for a variety of cell images by using different training examples and sample shape examples.

The use of autoregressive model for tracking shapes in motion can be found in [Blake et al., 1998, Blake and Isard, 1998]. However, the models were developed for explicit shape representations which is difficult to extend to higher dimensions. To alleviate this problem, we use the model for implicitly representing shapes. For segmentation, the use of shape prior can be found in [Rousson and Paragios, 2002, Paragios et al., 2003]. This approach can deal with noisy, occluded and missing data. However, the shape prior considered is static and is not suitable for applications such as tracking, where the shape changes over time. Therefore, we consider the dynamic models for implicitly represented shapes proposed in [Cremers, 2006]. It inherits some advantages of level set methods such as simple representation for contours of complex topology, while the use of low-dimensional formulation enhances the reliability of the model for predicting temporal shape prior. As shown in [Cremers, 2006], the model can successfully extract human in walking action. However, since the shape change of a cell on its full lifespan can be very dramatic, the model's ability to accurately predict the cell shape across different phases is questionable.

The remainder of this paper is organized as follows: In Section 2, we present a model approach to learn shape prior for tracking. In Section 3, we present an edge-based method for segmentation using prior. In Section 4, we present a Bayesian approach for cell phase identification. In Section 5, we show some experimental results of the proposed method. In Section 6, some concluding remarks are given.

2 Learning Shape Prior for Tracking

Recently, many works [Cremers, 2006, Zhou et al., 2008, Bresson et al., 2006, Chen et al., 2002] showed that the segmentation performance can be greatly improved by adding shape prior information. For instance, in many medical applications, a region-of-interest usually refers to entities with physical meanings. Hence, shape prior information is available to restrict the search of objects, which makes the segmentation problem more well-defined and the results more robust to noise. In our application, as cell shape may change dramatically, it can definitely be benefited from shape prior information. In this section, we demonstrate how to learn shape prior knowledge to enhance the segmentation performance and track cells.

2.1 Finite-dimensional curve representation

Given a sequence of N training (manually segmented) images. For each shape, we define the centroid as the center of mass and the orientation as the angle between the horizonal axis and the major axis of the ellipse that has the same second-moments as the shape. After a suitable transformation, all the shapes are centered and have 0° orientation. Their signed distance functions (SDFs) $\{\phi_1, \dots \phi_N\}$ are uniquely determined [Leventon et al., 2000]. Fig. 2 shows some training shape from each phase. The mean shape ϕ_0, is computed by taking the mean of the SDFs, $\phi_0 = \frac{1}{N}\sum \phi_i$. The n largest eigenmodes $\boldsymbol{\psi} = (\psi_1, \dots \psi_n)$ with $n \ll N$ are computed by Principal Component Analysis (PCA) [Duda et al., 2001]. Then each training

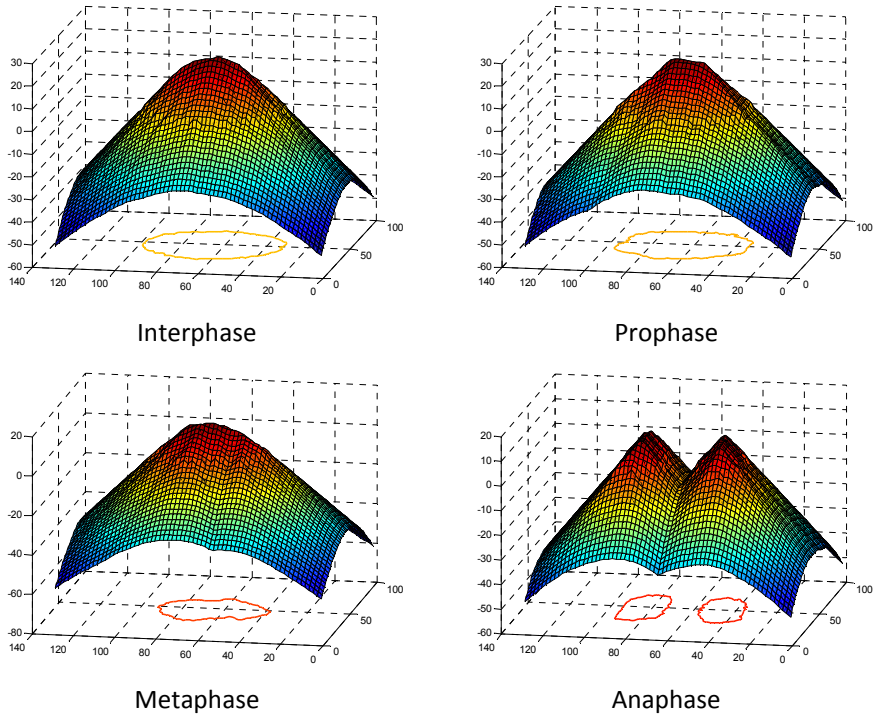

Figure 2: Sign distance function (SDF) and its zeroth level contour of a training shape (after transformation) in each phase.

shape can be approximated by a linear combination of the eigenmodes:

$$\phi_i(x) \approx \phi_0(x) + \sum_{j=1}^{n} \alpha_{ij}\psi_j(x), \tag{1}$$

where $\alpha_{ij} = \langle \phi_i - \phi_0, \psi_j \rangle \equiv \int (\phi_i(x) - \phi_0(x))\psi_j(x)\, dx$. This representation has been widely used for constructing shape priors [Leventon et al., 2000, Cremers, 2006]. The coefficients α_{ij} are the parameters for the level set formulation. As noticed in [Leventon et al., 2000], such a linear combination of SDFs is not a SDF in general. However, it is still smooth and preserves the common zero level sets of the original SDFs. These properties make it suitable for our application. Given an arbitrary shape ϕ (after a suitable transformation), it can be approximated by a shape vector of the form $\boldsymbol{\alpha}_\phi = (\langle \phi - \phi_0, \psi_1 \rangle, \ldots, \langle \phi - \phi_0, \psi_n \rangle)$. For the transformation parameters (translation and rotation), instead of using the absolute transformation θ, we use the incremental transformation $\Delta\theta$, i.e., difference between the current transformation and the previous transformation. Together with the shape parameters, a sequence of shapes can be represented by a sequence of combined vectors

$$\mathbf{v}_i = \begin{pmatrix} \boldsymbol{\alpha}_i \\ \Delta\theta_i \end{pmatrix}. \tag{2}$$

The main advantages of this representation are its simplicity and robustness. First, the low-dimensional shape representation can reduce the computational cost, comparing with using the whole signed distance function. Second, the model presented in the following section

will be more reliable when a lower dimensional representation is used because it can alleviate the over-fitting problem. In some related works on segmentation with shape prior [Bresson et al., 2006, Rousson and Paragios, 2002, Paragios et al., 2003], a scale parameter is also taken into account to handle objects with changing size. For cell tracking, the shape change is usually caused by phase transition in which no significant expansion and shrinkage is observed. Therefore, we do not include the scale parameter in our application. However, to apply the prior information learned from the training images, we first resize the testing images to have the same scale as the training images. We will elaborate this point more in Section 5.

2.2 Learning temporal dynamics of shape change

To learn the shape transitions, we model this process using an autoregressive model (AR) of order 2 [Neumaier and Schneider, 2001], i.e.,

$$\mathbf{v}_t = \mu + A_1\mathbf{v}_{t-1} + A_2\mathbf{v}_{t-2} + \eta, \tag{3}$$

where μ is the mean, η is zero-mean Gaussian noise with covariance Σ, and A_1, A_2 are the coefficient matrices. To estimate the model parameters $A_1, A_2, \mu, \eta, \Sigma$, we use a stepwise least squares method proposed in [Neumaier and Schneider, 2001]. With the model, we can estimate the parameters of the shape at time t, given the shape and transformation parameters $\{\mathbf{v}_1, \ldots, \mathbf{v}_{t-1}\}$ obtained from the previous shapes $\{\phi_1, \ldots, \phi_{t-1}\}$. In particular, we predict the shape vector $\mathbf{v}_t$ as $\tilde{\mathbf{v}}_t = \mu + A_1\mathbf{v}_{t-1} + A_2\mathbf{v}_{t-2}$. Since the estimation provides information about the shape and the location of the current object, this serves as a purpose of tracking embedded into the system. Figure 3 shows the approximation of a HeLa cell in each phase. Note that the cell shape and its approximated shape are similar, only that the approximated one is smoother than the original cell. It is because the less-smooth component has been removed in the low dimensional representation.

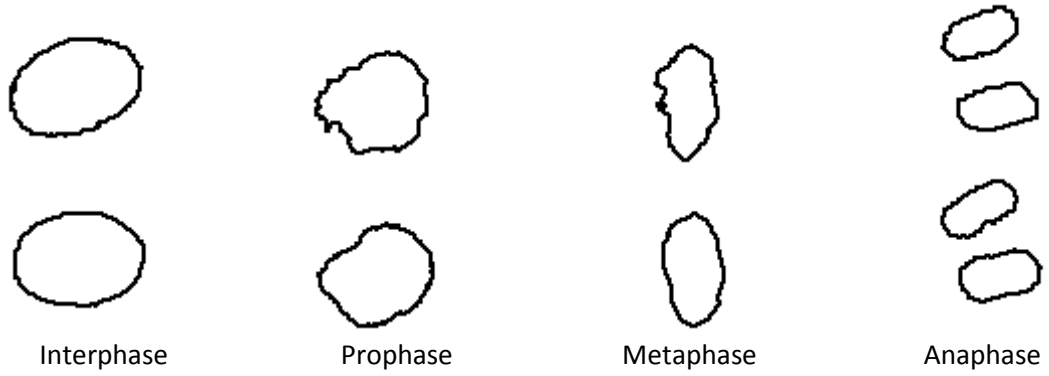

Figure 3: The approximation (below) of a cell (above) by the first six principal components.

3 Segmentation with shape prior initialization

Given an image $I_t : \Omega \to \mathbf{R}$ and a sequence of previous segmented images, our aim is to track the object in I_t making use of the information derived from the estimated shape vector

$\tilde{\mathbf{v}}_t$, which is often close to the object. In [Leventon et al., 2000, Tsai et al., 2001, Cremers, 2006], the estimated shape is used to incorporate as a prior shape into the segmentation model. This approach can improve the segmentation result by restricting the search of objects. However, as discussed in Section 1, restricting the searching space becomes impractical in our application since the shape change of a cell on its full lifespan can be very dramatic. Such a model is unable to predict the cell shape accurately across different phases (see Section 5). Therefore, to segment the object, we choose the edge-based active contour model proposed in [Li et al., 2010a] among many segmentation methods [Scherzer, 2011] with the estimated shape $\tilde{\mathbf{v}}_t$ served as an initialization. It is because this method inherits some advantages of level set methods such as simple representation for contours of complex topology and simple numerical computations on regular grids, while it has an intrinsic capability of maintaining regularity of the level set function. The objective is to find a level set function $\phi : \Omega \to \mathbf{R}$ such that the following energy functional $F(\phi)$ is locally minimized:

$$F(\phi) = a \int_\Omega p(|\nabla\phi|)\, dx + b \int_\Omega g\delta(\phi)|\nabla\phi|\, dx + c \int_\Omega gH(-\phi)\, dx \tag{4}$$

where $a, b > 0$ and $c \in \mathbf{R}$ are the coefficients of the three terms, p is a potential function, g is an edge indicator function, δ and H are the Dirac delta function and the Heaviside function respectively. Here, we use

$$p(s) = \begin{cases} \frac{1}{(2\pi)^2}(1-\cos(2\pi s)), & \text{if } s \le 1 \\ \frac{1}{2}(s-1)^2, & \text{if } s \ge 1, \end{cases} \qquad g = \frac{1}{1+|\nabla G_\sigma * I_t|^2} \tag{5}$$

where G_σ is a Gaussian kernel with a standard deviation σ. We expand the initial active contour to capture both the cell and some background area. We also set the coefficient c of the weighted area term to be positive to make the zero level set contour shrink in the level set evolution. The Dirac delta function δ and the Heaviside function H in Eq. (4) are respectively approximated by the following functions δ_ϵ and H_ϵ used in [Li et al., 2010a]:

$$\delta_\epsilon(x) = \begin{cases} \frac{1}{2\epsilon}[1+\cos(\frac{\pi x}{\epsilon})], & \text{if } |x| \le \epsilon \\ 0, & \text{if } |x| > \epsilon, \end{cases} \tag{6}$$

$$H_\epsilon(x) = \begin{cases} \frac{1}{2\epsilon}[1+\frac{x}{\epsilon}+\frac{1}{\pi}\sin(\frac{\pi x}{\epsilon})], & \text{if } |x| \le \epsilon \\ 1, & \text{if } x > \epsilon \\ 0, & \text{if } x < -\epsilon \end{cases} \tag{7}$$

To minimize the objective function (4), we apply gradient descent method. We denote by $\frac{\partial F}{\partial \phi}$ the (Gâteaux) derivative of F with respect to ϕ, i.e.,

$$\frac{\partial F}{\partial \phi} = -(a\mathrm{div}(d_p(|\nabla\phi|)\nabla\phi) + b\delta_\epsilon(\phi)\mathrm{div}\left(g\frac{\nabla\phi}{|\nabla\phi|}\right) + cg\delta_\epsilon(\phi)), \tag{8}$$

where $\mathrm{div}(\cdot)$ is the divergence operator and d_p is a function defined by

$$d_p(s) = \frac{p'(s)}{s}, \tag{9}$$

and δ_ϵ is an approximation of δ. Then, a single step of the gradient descent method computes the next iterate by the update $\phi^{k+1} = \phi^k - \Delta t \frac{\partial F}{\partial \phi}(\phi^k)$, where $\Delta t > 0$ is the step length parameter. The detailed numerical implementation can be found in [Li et al., 2010a]. Presumably, the contour stops at the object's boundary.

4 Cell phase identification

In this section, we identify the cell phase S_t based on the segmentation result obtained by the previous step. Here, we model this as a maximum-a-posteriori (MAP) problem. Such an approach has been widely used for modeling state transition [Zhou et al., 2008, 2009]. Given the current image I_t and the previous phases $S_{1:t-1} = \{S_1, \ldots, S_{t-1}\}$, we denote by $P(S_t|I_t, S_{1:t-1})$ the posterior probability of the current phase S_t. Then its maximizer S_t^* will be the optimal current phase. Based on the Bayesian formula, the expression can be rewritten as

$$P(S_t|I_t, S_{1:t-1}) = \frac{P(I_t|S_t, S_{1:t-1})P(S_t|S_{1:t-1})}{P(I_t|S_{1:t-1})} \propto P(S_t|S_{t-1})P(I_t|S_t). \tag{10}$$

The last expression is based on the assumptions that I_t and $S_{1:t-1}$ are uncorrelated and S_t depends only on the previous phase S_{t-1}. For simplicity, we consider the "left-right" model, i.e., transitions could happen only between consecutive phases. Also, we track the cell in one cycle. Moreover, the probabilities of all possible transitions from one phase are proportional to the fractions of occurrences. These assumptions can be expressed using the following matrix:

	I	P	M	A
I	a^{II}	a^{IP}	0	0
P	0	a^{PP}	a^{PM}	0
M	0	0	a^{MM}	a^{MA}
A	0	0	0	1

(11)

where I, P, M, A represent interphase, prophase, metaphase and anaphase, respectively. The transition probability is defined as

$$a^{ij} = \frac{\arctan(n^{ij}/\epsilon)}{\sum_k \arctan(n^{ik}/\epsilon)}, \tag{12}$$

where n^{ij} is the fraction of occurrences of transition i to j (i.e., number of occurrences of transition i to j/total number of frames in phase i) for $i, j \in \{I, P, M, A\}$, and $\epsilon > 0$ is a constant. Then, the transition matrix in two extreme cases are given in the following proposition.

Proposition 1. *When $\epsilon \to \infty$, the value a^{ij} in Eq.*(11) *approaches to n^{ij}. On the other hand, when $\epsilon \to 0$, the matrix becomes*

	I	P	M	A
I	$\frac{1}{2}$	$\frac{1}{2}$	0	0
P	0	$\frac{1}{2}$	$\frac{1}{2}$	0
M	0	0	$\frac{1}{2}$	$\frac{1}{2}$
A	0	0	0	1

(13)

The proposition can be derived directly from the facts that $\lim_{x\to 0} \tan(x)/x = 1$, and $\lim_{x\to\infty} \arctan(x) = \pi/2$.

For the likelihood function $P(I_t|S_t)$, we use the following similarity measure between the segmented shape ϕ and the sample shape ϕ_S associated with S where $S = \{I, P, M, A\}$:

$$P(I_t|S_t) \propto D(\phi, \phi_S) = \exp\left(-\sum_i \frac{|f_\phi^i - f_{\phi_S}^i|}{\sigma(f_i)}\right), \tag{14}$$

where f_ϕ is the shape and context features and $\sigma(f_i)$ is the standard deviations of the respective features over the set of training samples. Here, we use eight features suggested in [Zhou et al., 2009]: maximum intensity, minimum intensity, standard deviation of intensity, mean intensity, length of major axis, length of minor axis, perimeter and compactness (perimeter^2/(4$\pi\cdot$ Area)).

The phase information can be used to enhance the segmentation result. If the cell undergoes a phase transition, we repeat the segmentation step with the sample shape of the new (optimal) phase as an initial guess. The sample shape is first transformed to obtain the same centroid and orientation with the segmented shape. With this biological prior knowledge, the segmentation result could be further improved by this additional step. This will be illustrated in the experimental section.

We then use the final segmented shape to compute the shape vector $\mathbf{v}_t$ and use it for predicting the shape prior for the next image.

5 Experimental results

In the first part of this section, we evaluate the performance of the proposed method on tracking single cell empirically in various aspects: (1) temporal sampling rate, (2) comparison with other methods, (3) parameters for computing the transition matrix, and (4) dwelling time. In the second part, we evaluate the performance of tracking multiple cells from an image sequence of a group of cells. For all the tests except (3), the transition matrix in Eq. (13) is used.

For the first part of the experiments, some images capturing single cell movement are used. The cells are HeLa H2B-GFP cell line from [Elowe et al., 2010] and [Zhou et al., 2009] under various conditions. Frames were acquired at 3-minute intervals and 15-minute intervals respectively, with a time-lapse fluorescence microscopy. Each image is of 97×130 pixels. The images from [Elowe et al., 2010] are preprocessed to reduce the intensity of the cells touching the image borders. The cells are separated from the background by a global thresholding and the reduction is based on the distance between that pixel and the cells that are not on the image edge. For the images from [Zhou et al., 2009], we selected a subimage which captures a single cell movement. For the second part of the experiments, some images capturing multiple cell movement are used. The cells are HeLa H2B-EGFP cell line from [CMCB, 2013]. Frames were acquired at 3-minute intervals, with a time-lapse fluorescence microscopy.

To estimate the parameters of the model in Eq. (3), we manually segmented a sequence of 66 training images of a cell nucleus and computed the corresponding shape vectors and the eigenmodes ($n = 6$) described in Section 2. We used the estimated values for all the experiments. To obtain the initial values of $\mathbf{v}_1$ and $\mathbf{v}_2$ in Eq. (3) for the test sequence, we first manually segmented the first two test images. We then calculated the resizing factor as the ratio $\frac{\text{size of 1st training cell}}{\text{size of 1st test cell}}$ and resized all the test images accordingly. Next we computed the shape vectors $\mathbf{v}_1$ and $\mathbf{v}_2$ of the first two test images.

The percentage intersection between the manual and the computed segmentations, which is computed as the ratio $\frac{\text{no. of correctly labeled pixels}}{\text{total no. of pixels}}$, is used as a measure of segmentation accuracy and the mean accuracy with error bar is reported. The error bar indicates the standard deviation of the accuracy.

5.1 Sampling rate

In this test, we use a sequence of 45 images of a cell nucleus with 3-minute temporal resolution as the test set. From this sequence, we generate four other sequences by duplicating or skipping images to simulate sequences with higher or lower sampling rate respectively. Figure 4 shows the mean accuracy of the segmentation results vs. the temporal sampling rate and some resulting images in different phases. Observe that the accuracy remains high as the sampling rate is higher than 1. However, it deteriorates slightly when the rate is decreased. It shows that it is difficult to capture a dramatic change in shape due to low sampling rate stream. But the overall accuracy is still high. Thus, our algorithm is robust.

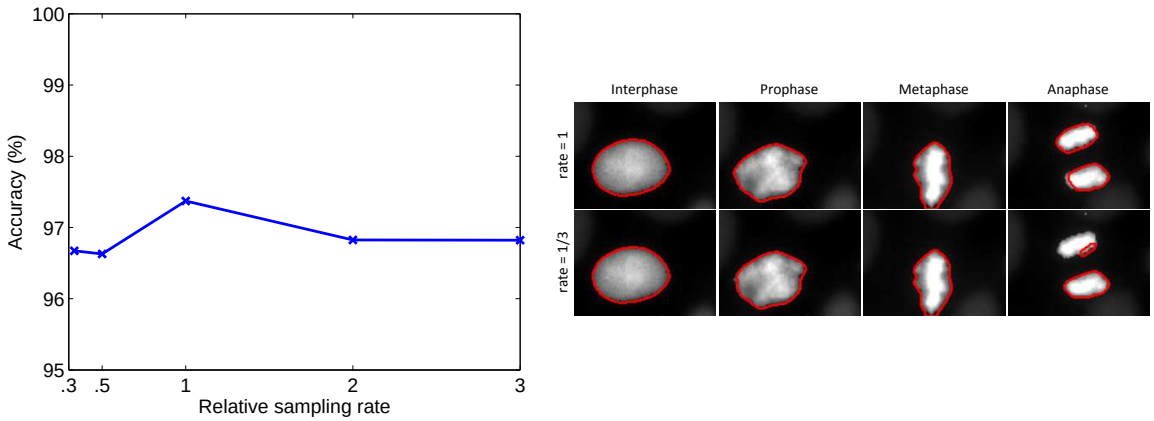

Figure 4: Mean accuracy vs. sampling rate and some resulting images in different phases with rate = $\{1, \frac{1}{3}\}$.

5.2 Comparing results from different methods

In this test, we first compare our method with the edge based segmentation model proposed in [Li et al., 2010a], which is indeed the component (C2) in our system, using the above image sequence. Hence, this test evaluates the essentiality of components (C1) and (C3). Figure 5 shows the mean accuracy of the segmentation results with different methods and some resulting images in different phases. Here, we use the final segmentation from one frame as the initialization of the next. Observe that the accuracies in the first three phases are comparable. However, the accuracy of Li's method in the anaphase deteriorates when both the steps (C1) and (C3) are absent and it finally lost track of the cell. Note that the morphological change from metaphase to anaphase is dramatic. Both the initialization learned from the dynamical model and assigned by phase identification improve significantly the results. We then compare with a shape prior embedded method proposed by Cremers [Cremers, 2006]. Note that our method outperforms Cremers's method in each phase. Observe that the shape of the resulting segmentation and the shape of the cell are quite different, which shows that the Cremers's method is unable to capture the shape change.

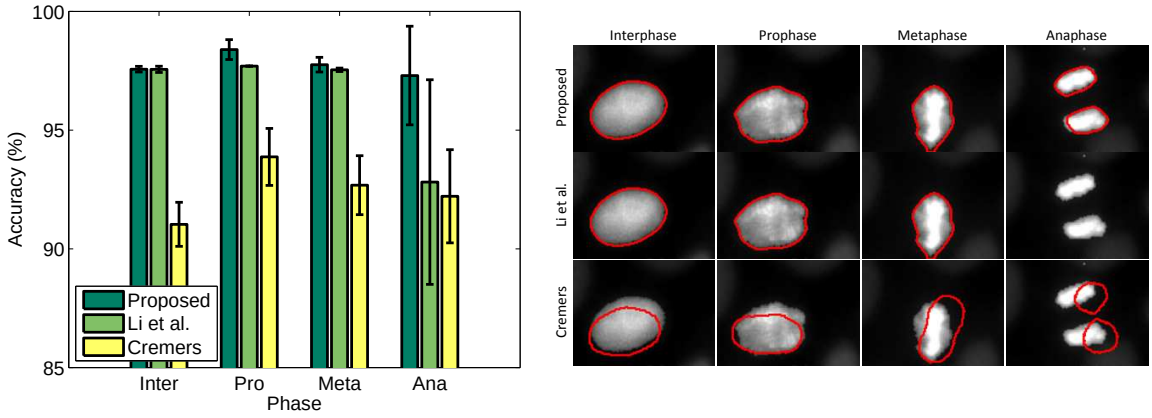

Figure 5: Mean accuracy with different methods and some resulting images in different phases.

5.3 Transition matrices with different parameters

In this test, we segment the above image sequence using different values of ϵ in Eq. (12) to compute the transition matrix in Eq. (11). Fig. 6 shows the mean accuracies of the segmentation results and the phase identification results vs. ϵ. Observe that both accuracies deteriorate when ϵ is increased. Note that the transition matrix in Eq. (11) approaches to the transition matrix in Eq. (13) when $\epsilon \to 0$. In this training set, the two matrices become equal when $\epsilon \leq 1 \times 10^{-5}$. On the other hand, when $\epsilon \geq 1 \times 10^{1}$, the method is unable to identify any phase transition and remains in the interphase. This situation is equivalent to the case when the step (C3) is absent. Hence, the segmentation accuracy also deteriorates, which is similar to the result of Li et al. [Li et al., 2010a] shown in Section 5.2.

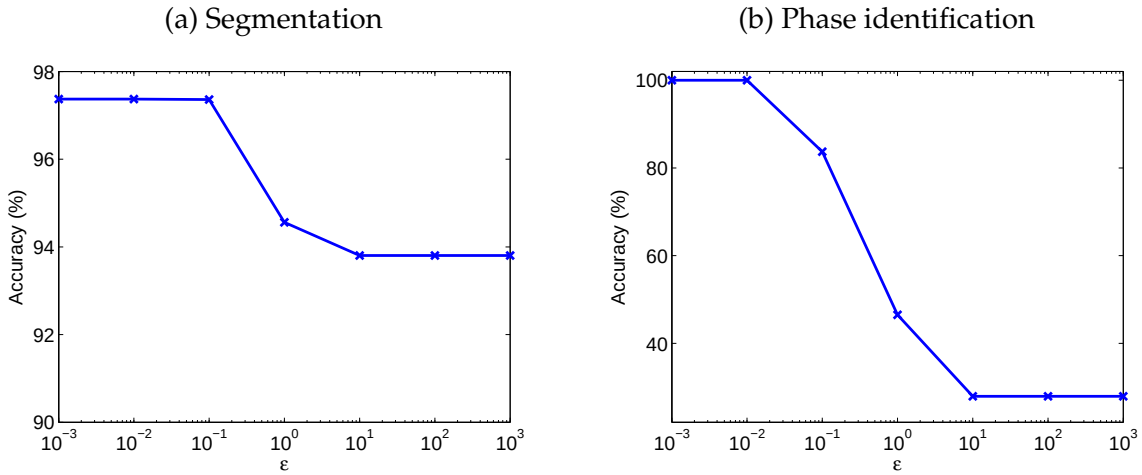

Figure 6: (a) Mean segmentation accuracy and (b) Mean phase identification accuracy with a wide range of ϵ in Eq. (12).

5.4 Image sequence with short dwelling time of prophase

In this test, we use two other sequences of 20 images of cell nuclei having different sampling rates (A: low, B: high). For these two sets, the cells have a very short dwelling time of prophase which makes phase identification more difficult. Figure 7 shows the mean accuracy and some resulting images from the two sets in different phases. Observe that a short dwelling time of prophase causes a miss of metaphase identification. The error also propagates to the next phase. The effect is shown in the result of set A. However, due of its higher sampling rate, there are more frames sampled in the metaphase in set B and hence is able to reduce the effect. Overall, the accuracy in the anaphase is lower than that in the other phases.

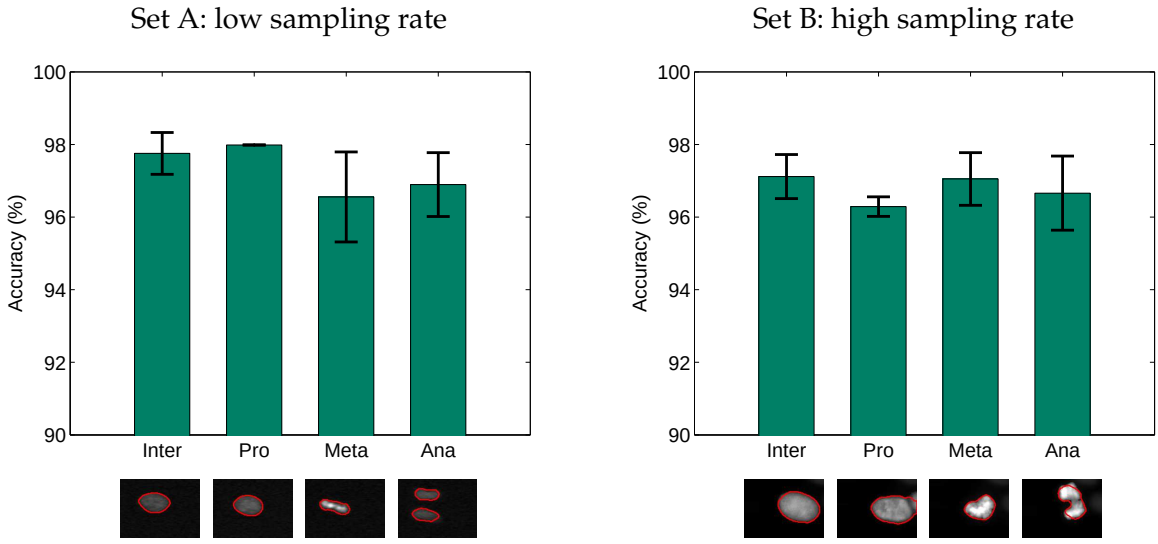

Figure 7: Mean accuracy and some resulting images in different phases on two sets of images with short prophase.

5.5 Multiple cell tracking

In this test, we evaluate the performance of our method on tracking individual cells in cell populations. For each individual cell, we use one level set function to track its trajectory on a subimage which has the same size as the training image and is centered on the coordinates of the centroid of that cell in the first test image. Fig. 8 shows (a) the mean accuracy in different phases, (b) the accuracy of individual cells over time and (c) some resulting images of some cells in different phases. Overall our method performs well and is able to track the cells. Note that the accuracy in anaphase is lower than that in the other phases. It is due to the fact that after cell division, the two daughter cells start growing and have considerable shape change. This scenario is observed in the resulting segmentation in anaphase. To deal with this, a new level set function can be used to track each newly born daughter cell.

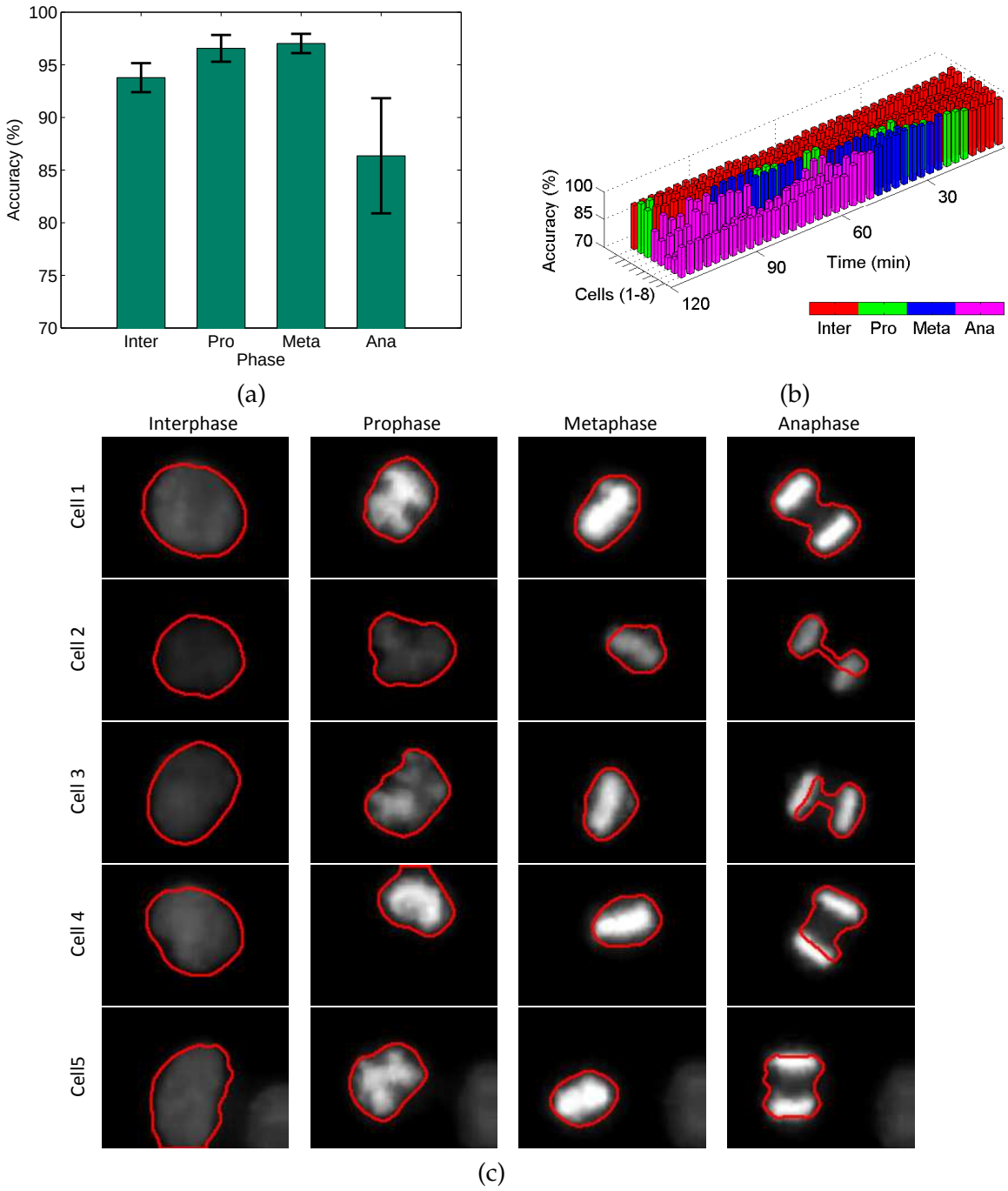

Figure 8: (a) Mean accuracy in different phases, (b) accuracy of individual cells over time, and (c) some resulting images of five cells in different phases.

6 Conclusion

In this paper, we introduced a three-component system for individual cell tracking in populations. This approach makes use of available biological prior knowledge to improve the performance of the process. On the other hand, it is very generic and can be applied for a large variety of cell images by using different training examples and sample shape examples. We tested our method on many different aspects and showed the robustness of our method. We also generalized the method to track multiple cells by using several level set functions. Future work is to further investigate the shape prior learning and the segmentation steps to deal with more advanced situations. In particular, we can consider learning a model for each phase by applying autoregression within each phase if the cell shape changes very dramatically. Also, when we segment cells from a dense population, a shape prior embedded approach can be considered. However, as observed in the experiment, the existing method of this approach is unable to capture the dramatic change of the shape and hence appropriate adjustment is necessary to improve its performance. Moreover, another promising future work is to optimize the performance of the integration approach to make it more practical.

Acknowledgement

This work was supported in part by the Biomedical Research Council of A*STAR (Agency for Science, Technology and Research), Singapore and by Academic Research Grant R-146-000-139-112 from the National University of Singapore, Singapore.

References

A. Blake and M. Isard. *Active Contours*. Springer, 1998.

A. Blake, B. Bascle, M. Isard, and J. MacCormick. Statistical models of visual shape and motion. *Philosophical Trans. of the Royal Society A*, 356:1283–1302, 1998.

X. Bresson, P. Vandergheynst, and J.-P. Thiran. A variational model for object segmentation using boundary information and shape prior driven by the Mumford-Shah functional. *Int. Journal of Computer Vision*, 68(2):145–162, 2006.

X. Chen, X. Zhou, and S. Wong. Automated segmentation, classification, and tracking of cancer cell nuclei in time-lapse microcopy. *IEEE Trans. on Biomedical Engineering*, 53(4): 762–766, 2006.

Y. Chen, H.D. Tagare, S. Thiruvenkadam, F. Huang, D. Wilson, K.S. Gopinath, R.W. Briggsand, and E.A. Geiser. Using prior shapes in geometric active contours in a variational framework. *Int. Journal of Computer Vision*, 50(3):315–328, 2002.

The University of Warwick CMCB. Mitosis in human HeLa cells. Website, 2013. URL `http://mechanochemistry.org/movies/`. (Date of last access: 1 April 2013).

D. Cremers. Dynamical statistical shape priors for level set-based tracking. *IEEE Trans. on Pattern Analysis and Machine Intelligence*, 28(8):1262–1273, 2006.

R. Duda, P. Hart, and D. Stock. *Pattern Classification*. John Wiley & Sons, NY, 2001.

O. Dzyubachyk, W. A. van Cappellen, J. Essers, W.J. Niessen, and E. Meijering. Advanced level-set based cell tracking in time-lapse fluorescence microscopy. *IEEE Trans. on Medical Imaging*, 29(3):852–867, 2010.

S. Elowe, K. Dulla, A. Uldschmid, X. Li, Z. Dou, and E.A. Nigg. Uncoupling of the spindle-checkpoint and chromosome-congression functions of BubR1. *Journal of Cell Science*, 123: 84–94, 2010.

G. Lahav, N. Rosenfeld, A. Sigal, N. Geva-Zatorsky, A.J. Levine, M.B. Elowitz, and U. Alon. Dynamics of the p53-mdm2 feedback loop in individual cells. *Nature Genetics*, 36(2):147–150, 2004.

Y. N. Law and H. K. Lee. Level set based tracking for cell cycle analysis using dynamical shape prior. In *Proc. Medical Image Understanding and Analysis*, pages 137–142, 2012.

M. Leventon, W. Grimson, and O. Faugeras. Statistical shape influence in geodesic active contours. In *Proc. Computer Vision and Pattern Recognition*, pages 316–323, 2000.

C. Li, C. Xu, C. Gui, and M.Fox. Distance regularized level set evolution and its application to image segmentation. *IEEE Trans. on Image Processing*, 19(12):3243–3254, 2010a.

F. Li, X. Zhou, J. Ma, and S. Wong. Multiple nuclei tracking using integer programming for quantitative cancer cell cycle analysis. *IEEE Trans. on Medical Imaging*, 29(1):96–105, 2010b.

H. Lodish, A. Berk, S. Zipursky, P. Matsudaira, D. Baltimore, and J. Darnell. *Molecular Cell Biology*, chapter 13. W.H. Freeman & Co., 2000.

A. Neumaier and T. Schneider. Estimation of parameters and eigenmodes of multivariate autoregressive models. *ACM Trans. on Mathematical Software*, 27(1):27–57, 2001.

N. Paragios, M. Rousson, and V. Ramesh. Non-rigid registration using distance functions. *Computer Vision and Image Understanding*, 89(2-3):142–165, 2003.

M. Rousson and N. Paragios. Shape priors for level set representations. In *Proc. European Conference on Computer Vision*, pages 78–92, 2002.

O. Scherzer. *Handbook of Mathemtical Methods in Imaging*. Springer, 2011.

A. Tsai, A.J. Yezzi, , and A.S. Willsky. Curve evolution implementation of the mumford-shah functional for image segmentation, denoising, interpolation, and magnification. *IEEE Trans. on Image Processing*, 10(8):1169–1186, 2001.

X. Zhou and S. Wong. Informatics challenges of high-throughput microscopy. *IEEE Signal Processing Magazine*, 23(3):63–72, 2006.

X. Zhou, X. Li, and W. Hu. Level set tracking with dynamical shape priors. In *Proc. Int. Conference on Image Processing*, pages 1540–1543, 2008.

X. Zhou, F. Li, J. Yan, and S. Wong. A novel cell segmentation method and cell phase identification using markov model. *IEEE Trans. on Infomation Technology in Biomedicine*, 13(2): 152–157, 2009.